RSC Advances

PAPER

View Article Online
View Journal | View Issue

Cite this: *RSC Adv.*, 2019, **9**, 20963

Hollow Cu-doped NiO microspheres as anode materials with enhanced lithium storage performance†

Qiwen Hu,[a] Wenyao Li,*[a] Dina Ibrahim Abouelamaiem,[b] Chaoting Xu,[c] Haishun Jiang,[a] Weihua Han*[d] and Guanjie He*[b]

Received 20th May 2019
Accepted 1st July 2019

DOI: 10.1039/c9ra03780b

rsc.li/rsc-advances

Doping is an effective way to optimize the properties of electrode materials. In this study, hollow Cu-doped NiO microspheres were obtained *via* the hydrothermal method, in which the microspheres were aggregated from nanoparticles. Compared with the original NiO electrode, the Cu-doped NiO electrode exhibits prominent initial capacity (1180 *vs.* 900 mA h g^{-1}) and better rate capability (80% *vs.* 30% retention) as anode materials. The superior electrochemical properties could be attributed to the enhanced conductivity by Cu doping.

1. Introduction

Recently, with the depletion of fossil fuels, and the utilization of renewable energy, developing the corresponding energy storage devices has become more and more vital.[1] Next-generation lithium ion batteries (LIBs) are widely applied in portable electronic devices due to their excellent energy density, long cycling life, and good environmental compatibility.[2–5] However, the widely used conventional graphite anode material has a low Li^+ diffusion coefficient and inferior theoretical specific capacity (372 mA h g^{-1}).[6,7] Moreover, the operating potential of graphite is below 0.2 V (*vs.* Li/Li^+) and lithium dendrites will grow on the anode surface if the state is overcharged, which can cause serious safety issues.[8] Therefore, the challenge continues for searching for promising alternative anode materials that exhibit higher performances.[9–11]

Transition metal oxides (TMOs), especially nickel oxide (NiO), are showed increasing solicitude as anode materials, which is attributed to its outstanding energy density and its high capacity that is at least twice of graphite.[12] Unfortunately, NiO anode materials can not suffer grievous volume expansion, which gives collapses the material structure, thus not maintaining long cycling stability.[13–15] In addition, due to the inferior conductivity and volume strain of the NiO crystal, the electrochemical properties also decrease sharply.[16,17] Appropriate doping of metal ions can be a practical method to improve the electronic conductivity.[18–20] In recent years, Thi *et al.*[21] reported a Co-doped NiO nanoparticle, which was prepared *via* polyol-based solvothermal method, the capacity maintained a value of 1017 mA h g^{-1} after 50 cycles at 0.1 C. Chen *et al.*[22] produced Cu-doped CoO hierarchical structures electrode material by hydrothermal reaction, and the capacity maintained was 800 mA h g^{-1} after 80 cycles at 0.5 C. Li *et al.*[23] reported the production of Li-doped NiO for anode materials *via* spray pyrolysis, whereby the electrode revealed outstanding electrochemical property with the capacity of 907 mA h g^{-1} after 100 cycles at 0.5 C. This portend that controlled chemical doping of metals has also been proven to strengthen the electrochemical properties of NiO electrode for LIBs. In addition, the ionic radius of Ni^{2+} (0.55 Å) is similar to Cu^{2+} (0.57 Å), where there is only small lattice expansion of NiO when the Cu^{2+} take the place of Ni^{2+}.[24] Besides, it is reported that the first-principle calculations and experiment demonstrated that the doping of Cu can change the orientation of crystal growth and significantly enhance the stability of CoO,[25] and Nam *et al.* confirmed that Cu-doped dual phase $Li_4Ti_5O_{12}$–TiO_2 composite can reach a great improvement in the electrochemical performance.[26] However, there are infrequent reports for Cu doped NiO anode material for LIBs.

Herein, Cu-doped NiO hollow microspheres aggregated from 50–100 nanoparticles were synthesized *via* one-step hydrothermal way. As anode material, an upper capacity of 1180 mA h g^{-1} was achieved, compared to the original NiO microspheres (900 mA h g^{-1}). Moreover, the Cu-doped NiO electrode maintains 80% capacity through a varied current density measurement, while the original NiO electrode retains

[a]*School of Material Engineering, Shanghai University of Engineering Science, Shanghai 201620, China. E-mail: liwenyao314@gmail.com*

[b]*Materials Chemistry Centre, Department of Chemistry, University College London, 20, Gordon Street, London WC1H 0AJ, UK. E-mail: g.he@ucl.ac.uk*

[c]*State Key Laboratory for Modification of Chemical Fibers and Polymer Materials, College of Materials Science and Engineering, Donghua University, Shanghai 201620, China*

[d]*School of Physical Science and Technology, Lanzhou University, Lanzhou 730000, China. E-mail: hanwh@lzu.edu.cn*

† Electronic supplementary information (ESI) available: The SEM images, EDS, CV curves and galvanostatic discharge of the NiO and Cu-doped NiO samples. See DOI: 10.1039/c9ra03780b

only 30% of the initial capacity. Thus, the Cu-doping is a practical strategy to strengthen the electrochemical properties of NiO, demonstrating enormous potential as electrode materials for LIBs.

2. Experimental section

2.1 Preparation process

NiO was prepared *via* a hydrothermal way. Firstly, 4 mmol $Ni(NO_3)_2 \cdot 6H_2O$, 30 mmol urea and 2 g cetyltrimethyl ammonium bromide were dissolved in 70 mL deionized water to form a pellucid liquor. The mix was then stirred for 2 h and transferred into a 100 mL autoclave. The solution was maintained at 70 °C with the soaking time of 24 h, followed by heating to 120 °C with the soaking time of 12 h. The sediment was obtained by centrifugation after the liquor come to room temperature, and washed alternately with three times of ethanol and three times of deionized water. Finally, the intermedium was calcined at 600 °C in N_2 atmosphere with the soaking time of 2 h to obtain NiO.

Analogously, the Cu-doped NiO was obtained with a mole ratio of Ni : Cu = 0.95 : 0.05, *i.e.*, 0.2 mmol $Cu(NO_3)_2 \cdot 3H_2O$ was added to the above hybrid liquor. Following the same heating and washing procedure for the preparation of NiO, Cu-doped NiO samples were obtained.

2.2 Characterizations

The products were characterized using a PANalytical X' Pert X-ray diffractometer (Holland), a field emission scanning electron microscope (SEM, S-4800, equipped with EDS), and a transmission electron microscope (TEM, JEM-2010F). X-ray photoelectron spectroscopy (XPS, Thermo VG Scientific).

2.3 Electrochemical measurements

The electrochemical property of the products was estimated using coin cells (CR2032, Hefei Ke Jing Materials Technology Co., LTD.). The working electrode was prepared using 70 wt% active material (NiO and Cu-doped NiO), 20 wt% acetylene carbon black (conductive agent), and 10 wt% polyvinylidene fluoride (PVDF) binder. And 1 M $LiPF_6$ in ethylene carbonate (EC) and diethyl carbonate (DEC) (1 : 1 by volume) was served as the electrolyte. The electrochemical property was evaluated by NEWARE-BTS battery tester and Autolab (PGSTAT302N potentiostat).

3. Results and discussion

The crystalline structure and phase purity of the original NiO and Cu-doped NiO were characterized by XRD. As shown in Fig. 1, both of the NiO and Cu-doped NiO patterns reveal five distinct peaks at 2θ degrees of 37.2, 43.3, 62.8, 75.4 and 79.3, which could be discovered to (111), (200), (220), (311) and (222) lattice planes of cubic phase NiO (JCPDS no.73–1523) as shown in Fig. 1. Interestingly, there are four small peaks obtained from the XRD pattern of Cu-doped NiO sample (marked with a blue star). The diffraction peaks at 36.6, 42.6, 61.8 and 74.0 degrees

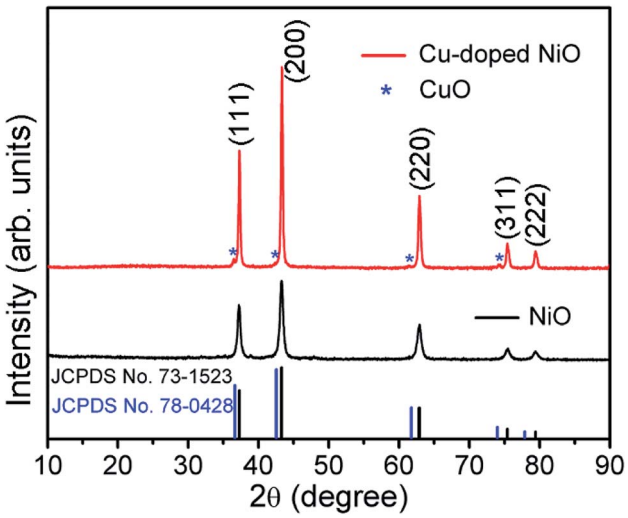

Fig. 1 XRD patterns of NiO and Cu-doped NiO.

could be respectively allotted to the (111), (200), (220) and (311) lattice planes, respectively indexed to the cubic phase of CuO (JCPDS no. 78–0428). As the peaks are weak, a more detailed analysis was carried out to confirm the success of Cu doping, as detailed later.

The Fig. 2 displays the morphology of the original NiO products using SEM and TEM techniques. A single NiO demonstrate a micro-spherical morphology with diameter of ~1–3 μm (SEM image of Fig. S1† displays the large scale NiO microspheres). The enlarged SEM image (Fig. 2b) shows that the microsphere is aggregated from a large number of nanoparticles. It is demonstrated that the nanoparticles are not of regular morphology and have a particle size of ~20–50 nm (Fig. 2c). Fig. 2d is the high resolution TEM (HRTEM) image of a single NiO particle, showing the interplanar d-spacing of 0.24 that matches to the (111) plane of NiO.

After doping Cu on NiO, the products are also characterized, Fig. 3a and b show the SEM images of Cu-doped NiO (Fig. S1b† shows the corresponding lower magnification SEM image of

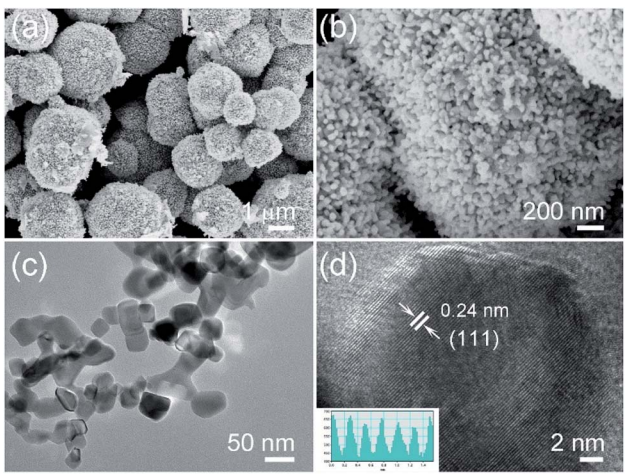

Fig. 2 (a and b) Low and enlarged SEM images of NiO, (c) TEM image of NiO nanoparticles, (d) HRTEM image of NiO.

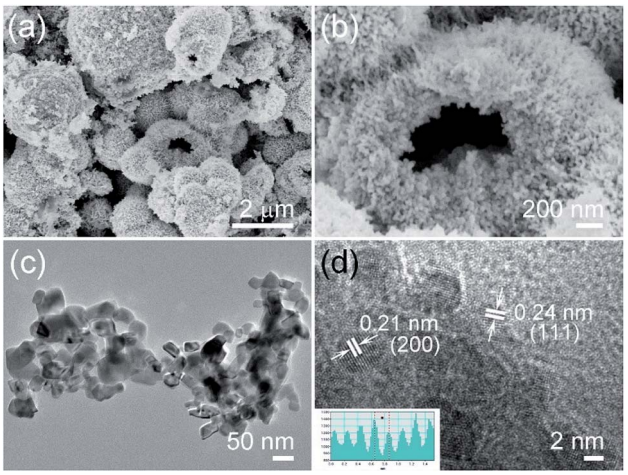

Fig. 3 (a and b) Low-resolution and enlarged SEM images of Cu-doped NiO, (c) TEM image of Cu-doped NiO nanoparticles and (d) HRTEM image of CuO phase in NiO.

large scale products). The morphology is similar to the NiO sample, which consists of microspheres aggregated from small nanoparticles. Interestingly, the Cu-doped NiO microspheres are of a hollow structure. The corresponding EDS pattern in Fig. S2† confirm the existence of Ni, Cu and O in the doped material. Fig. 3c shows the Cu-doped NiO nanoparticles with irregular shape and a particle size (50–100 nm) which is larger compared to undoped NiO nanoparticles. From the HRTEM of the Cu-doped NiO (Fig. 3d), it is observed that some small particles and idiosyncratic lattice structure exist, except for the interplanar *d*-spacing of 0.24 that correspond to the (111) plane of cubic phase NiO, the *d*-spacing of 0.21 is correspond to the (200) plane of cubic phase CuO, which matches well with the XRD.

Owing to the weak intensity of the CuO phase in Cu-doped NiO XRD pattern, XPS spectra of Cu-doped NiO have been carried to certify the impact of Cu doping in the valence state of NiO (Fig. 4). Fig. 4a displays the full XPS spectrum of Cu-doped NiO samples, which suggests the presence of Ni, Cu and O. The XPS high-resolution spectra are further analyzed and presented in Fig. 4b. The Ni2p signals at the location of ~853.5 and ~855.2 eV is due to $2p_{3/2}$ peaks, and the additional peak located at around 860.7 eV is matched to the satellite of $Ni2p_{3/2}$. The location of ~871.5 eV and 879.5 eV are due to $2p_{1/2}$ and satellite of $Ni2p_{1/2}$, respectively.[27,28] Fig. 4c shows the matching 2p core level XPS spectrum of the Cu in the doped sample. The recorded spectrum displays the Cu2p signals at the location of ~933.5 and 953.5 eV that are matched to $Cu2p_{3/2}$ and $Cu2p_{1/2}$, respectively. The other peaks at 941.3, 943.6 and 962.2 eV are ascribed to the strong Cu^{2+} satellites.[29] The O1s spectrum is detected in Fig. 4d, and the peaks at 531.2 and 529.3 eV could be corresponded to the exist of oxygen ions existing in the Cu-doped NiO.[30]

To confirm the properties of Cu-doped NiO microspheres, the Cu-doped NiO microspheres were fabricated as an electrode and at the electrochemical measurements were conducted using the Autolab electrochemistry workstation. Fig. 5a shows the CV of the 2nd cycle of both the Cu-doped NiO and general NiO (the first 3 cycles are shown in Fig. S3 and S4†). The loops of Cu-doped NiO are much larger than the general NiO, which indicates that the capacity of Cu-doped NiO electrode is superior compared to the general one. In addition, except for the strong peak at ~1.1 V which is put down to the reaction of NiO, a weak reduction peak exists in the CV of Cu-doped NiO electrode at 1.65 V. The latter could be attributed to the electrochemical reaction of small amounts of Cu doping.[24] Based on the analysis of the CV curves and previous reports, the Li reactions for Cu-doped NiO microspheres could take place as follows:[24]

$$NiO + 2Li^+ + 2e^- \Leftrightarrow Ni + Li_2O$$

$$CuO + 2Li^+ + 2e^- \Leftrightarrow Cu + Li_2O$$

GCD tests were performed to determine the effect of the Cu-doping of NiO electrode on the specific capacity values. As

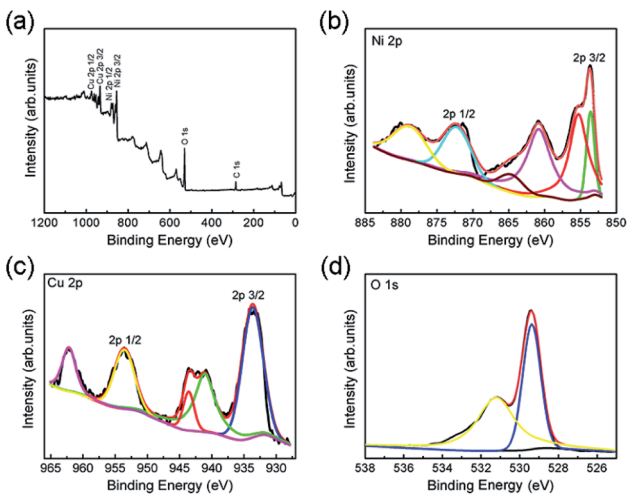

Fig. 4 (a) XPS wide spectrum of the obtained Cu-doped NiO sample. The XPS high-resolution spectra of (b) Ni2p, (c) Cu2p and (d) O1s.

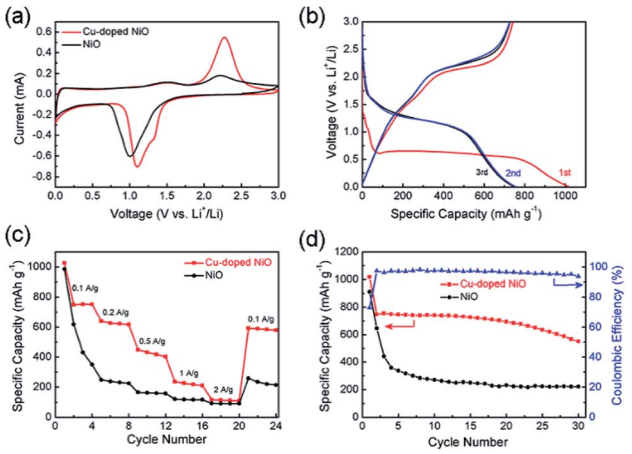

Fig. 5 (a) CV curves of Cu-doped NiO and original NiO at 0.1 mV s^{-1} scan rate, (b) galvanostatic charge–discharge (GCD) profiles for first three cycles of Cu-doped NiO at 100 mA g^{-1}, (c) rate capability and (d) cycling performances for NiO and Cu-doped NiO.

shown in Fig. 5b, the GCD curves for the 1st, 2nd and 3rd cycles of the Cu-doped NiO electrode at 100 mA g^{-1}. A wide voltage plateau is discerned in the initial discharge curve between 0.5 V and 0.7 V. Moreover, there is a small plateau in the 1st cycle at ~1.1 V compared with the un-doped electrode (Fig. S5†), which is put down to the influence of Cu doping.[24] The initial charge capacity for the Cu-doped NiO electrodes is ~1180 mA h g^{-1}, which is much higher compared to the NiO electrode (~900 mA h g^{-1}).

The rate property of the NiO and Cu-doped NiO electrodes is shown in Fig. 5c, which demonstrates the better rate performance of Cu-doped NiO electrode than that of the NiO electrode at 0.1, 0.2, 0.5, 1 and 2 A g^{-1}. The Cu-doped NiO displays higher discharge capacity than the general one, followed by capacity decay with an increase in the current density. In addition, when the current density of Cu-doped NiO electrode was reduced again to 0.1 A g^{-1} after cycling, the capacity obtains ~80%, which outperforms the NiO electrode (~30%).

Fig. 5d presents the cycling property of NiO and Cu-doped NiO at 100 mA g^{-1} for 30 cycles. The capacity of Cu-doped NiO was calculated to be ~1180 mA h g^{-1} in the first cycle, and maintaining capacity values of ~540 mA h g^{-1} after 30 cycles. However, the property of the NiO severely deteriorated, whereby the capacity value decreased to ~210 mA h g^{-1} after 30 cycles starting with initial capacity of ~900 mA h g^{-1} in the 1st cycle. The significant increase in the capacities obtained with the Cu-doping of the NiO electrode is attributed to the increasing conductivity upon Cu-doping of the electrode.[22] Moreover, the initial coulombic efficiency of Cu-doped NiO is 75%, and the efficiency remains above 90% after the first cycle, indicating a high and fast accessibility for lithium insertion/extraction into/from Cu-doped NiO hollow microspheres.

The Nyquist plots of Cu-doped NiO and un-doped NiO are presented in Fig. 6. The intersection point on the real axis is matched the electrolyte resistance. The semicircle area in the high frequency is the representative of R_{ct} in the electrode/electrolyte interface, and the inclined line in low frequency region is matched to Warburg impedance.[22] A semicircle of smaller diameter was obtained after comparing with the NiO one, whereby the R_{ct} of the Cu-doped NiO microspheres was evaluated to be 68 Ω, while that of NiO sample to be 148 Ω. The decrease in the R_{ct} upon doping the NiO with Cu can be put down to the more effective ion and electron transfer.[23] This proves that the Cu-doped NiO electrode demonstrates enhanced electrode reaction kinetics of the lithium ion battery.

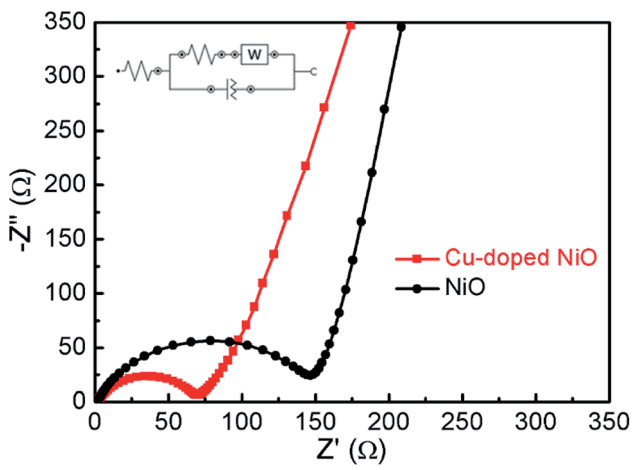

Fig. 6 Electrochemical impedance spectra of the NiO and Cu-doped NiO.

4. Conclusion

Hollow Cu-doped NiO microspheres were prepared *via* a facile one-step hydrothermal way. The hollow structure dramatically increases the contact of electrode and electrolyte, and effectively remit the volume expansion during the charge/discharge process. The Cu-doped NiO microspheres electrode possesses an outstanding high initial capacity of ~1180 mA h g^{-1} at 100 mA g^{-1} with enhanced rate property (80% retention after varied current densities measurement) compared to un-doped NiO electrodes. The splendid electrochemical property of the Cu-doped NiO is mainly ascribed to (i) the doping of Cu element causes the material to transform into a hollow structure during the synthesis process, which greatly buffers the bulk stress during lithiation; (ii) the improved electrical conductivity of electrode materials after Cu doping, which is a promising way to satisfy the requirements of high-performance Li-ion batteries.

Conflicts of interest

There are no conflicts to declare.

Acknowledgements

The work is funded by the National Natural Science Foundation of China (51602193), Shanghai "Chen Guang" project (16CG63), the Fundamental Research Funds for the Central Universities (WD1817002), and the Talent Program of Shanghai University of Engineering Science, Science and Technology Facilities Council for STFC/MDC Futures Early Career Award.

Notes and references

1 L. F. Chen, Y. Feng, H. W. Liang, Z. Y. Wu and S. H. Yu, *Adv. Energy Mater.*, 2017, **17**, 1700828.
2 B. Huang, Z. F. Pan, X. Y. Su and L. An, *J. Power Sources*, 2018, **399**, 274.
3 W. Li, B. Zhang, R. Lin, S. M. Ho-Kimura, G. He, X. Zhou, J. Hu and I. P. Parkin, *Adv. Funct. Mater.*, 2018, **28**, 1705937.
4 G. He, X. Han, R. Zou, T. Zhao, Z. Weng, S. M Ho-Kimura, Y. Lu, H. Wang, Z. Guo and I. P. Parkin, *Adv. Funct. Mater.*, 2017, **27**, 1604903.
5 B. Moradi and G. G. Botte, *J. Appl. Electrochem.*, 2016, **46**, 123.
6 P. C. Zhang, T. Yuan, Y. P. Pang, C. X. Peng, J. H. Yang, Z. F. Ma and S. Y. Zheng, *J. Electrochem. Soc.*, 2019, **166**, A5489.
7 A. Sameen, R. Muhammad, H. Y. Liu, R. Iqra and A. Hurria, *Carbon Lett.*, 2018, **28**, 1.

8 L. F. Shen, X. G. Zhang, E. Uchaker, C. Z. Yuan and G. Z. Cao, *Adv. Energy Mater.*, 2012, **2**, 699.
9 M. S. Whittingham, *Science*, 1976, **192**, 1126.
10 M. D. Bhatt and C. O'Dwyer, *Phys. Chem. Chem. Phys.*, 2015, **17**, 4799.
11 Z. L. Xiong, Y. S. Yun and H. J. Jin, *Materials*, 2013, **6**, 1138.
12 B. Varghese, M. V. Reddy, Y. W. Zhu, C. S. Lit, T. C. Hoong, G. V. S. Rao, B. V. R. Chowdari, A. T. S. Wee, C. T. Lim and C. H. Sow, *Chem. Mater.*, 2008, **20**, 3360.
13 D. Xie, Q. M. Su, W. W. Yuan, Z. M. Dong, J. Zhang and G. H. Du, *J. Phys. Chem. C*, 2013, **117**, 24121.
14 Y. Q. Zou and Y. Wang, *Nanoscale*, 2011, **3**, 2615.
15 Q. Li, Y. J. Chen, T. Yang, D. N. Lei, G. H. Zhang, L. Mei, L. B. Chen, Q. H. Li and T. H. Wang, *Electrochim. Acta*, 2013, **90**, 80.
16 D. Xie, W. W. Yuan, Z. M. Dong, J. Zhang and G. H. Du, *Electrochim. Acta*, 2013, **92**, 87.
17 L. Cao, D. X. Wang and R. Wang, *Mater. Lett.*, 2014, **132**, 357.
18 X. Li, Y. Xiang, B. Qu and S. Su, *Mater. Lett.*, 2017, **203**, 1.
19 F. Chen, J. Wang, L. Huang, H. Bao and Y. Shi, *Chem. Mater.*, 2016, **28**, 608.
20 W. Ding, X. Wang, H. Peng, Z. Peng and B. Dong, *Mater. Res. Bull.*, 2013, **48**, 4704.
21 T. V. Thi, A. K. Rai, J. Gim and J. Kim, *J. Power Sources*, 2015, **292**, 23.
22 C. C. Chen, Y. N. Huang, H. Zhang, X. F. Wang, Y. J. Wang, L. F. Jiao and H. T. Yuan, *J. Power Sources*, 2016, **314**, 66.
23 Y. Li, X. H. Li, Z. X. Wang, H. J. Guo and T. Li, *Ceram. Int.*, 2016, **42**, 14565.
24 H. Chen, C. L. Li, N. Li, X. K. Xiang and Z. L. Hu, *Micro Nano Lett.*, 2013, **8**, 544.
25 C. H. An, Y. J. Wang, Y. N. Huang, Y. N. Xu, L. F. Jiao and H. T. Yuan, *Nano Energy*, 2014, **10**, 125.
26 K. M. Nam, Y. C. Choi, S. C. Jung, Y. Kim, M. R. Jo, S. H. Park, Y. M. Kang, Y. K. Han and J. T. Park, *Nanoscale*, 2012, **4**, 473.
27 L. Cao, D. Wang and R. Wang, *Mater. Lett.*, 2014, **132**, 357.
28 Y. R. Ren, H. M. Wei, X. B. Huang, B. Yang and J. N. Ding, *Int. J. Electrochem. Sci.*, 2014, **9**, 7206.
29 S. Tougaard and D. Tahir, *J. Phys.: Condens. Matter*, 2012, **24**, 175002.
30 W. Guo, W. Sun and Y. Wang, *ACS Nano*, 2015, **9**, 11462.